DMD Fast Forward. Published on August 30, 2021 as DOI: 10.1124/dmd.121.000571
This article has not been copyedited and formatted. The final version may differ from this version.

The IL-6/STAT3/CTH axis deciphers the transformation between the sensitive and resistant phenotypes of breast cancer cells

Zhaoyi Tan[1#], Chun Ge[2,3#], Dong Feng[1,4#], Chen Xu[1#], Bei Cao[5], Yuan Xie[1], Honghao Zhou[6,*], Guangji Wang[1,*], Jiye Aa[1,*]

[1]Key Laboratory of Drug Metabolism and Pharmacokinetics, State Key Laboratory of Natural Medicines, China Pharmaceutical University, Nanjing, 210009, China

[2]Department of Pharmacy, Nanjing First Hospital, Nanjing Medical University, Nanjing, 210006, China

[3]Department of Clinical Pharmacy, School of Basic Medicine & Clinical Pharmacy, China Pharmaceutical University, Nanjing, 210009, China

[4]Nanjing Southern Pharmaceutical Technology Co. Ltd., Nanjing, 211100, China

[5]Phase I Clinical Trials Unit, The Affiliated Drum Tower Hospital of Nanjing University Medical School, Zhongshan Road 321#, Gulou district, Nanjing 210008, China

[6]Pharmacogenetics Research Institute, Xiang-Ya School of Medicine, Central South University, Changsha, 410078, China

# These authors contributed equally to this work.

* To whom correspondence should be addressed.

Honghao Zhou, Pharmacogenetics Research Institute, Xiang-Ya School of Medicine, Central South University, Changsha. E-mail: hhzhou@public.cs.hn.cn

Guangji Wang, Key Laboratory of Drug Metabolism and Pharmacokinetics, State Key Laboratory of Natural Medicines, China Pharmaceutical University, Nanjing. E-mail: guangjiwang@hotmail.com

Jiye Aa, Key Laboratory of Drug Metabolism and Pharmacokinetics, State Key Laboratory of Natural Medicines, China Pharmaceutical University, Nanjing. E-mail: jiyea@cpu.edu.cn

DMD Fast Forward. Published on August 30, 2021 as DOI: 10.1124/dmd.121.000571
This article has not been copyedited and formatted. The final version may differ from this version.

Modulation of P-gp and drug resistance

Zhaoyi Tan[1#], Chun Ge[2,3#], Dong Feng[1,4#], Chen Xu[1#], Bei Cao[5], Yuan Xie[1], Honghao Zhou[6,*], Guangji Wang[1,*], Jiye Aa[1,*]

The number of text pages, 31

The number of tables, 0

The number of figures, 7

The number of Supplementary tables, 1

The number of Supplementary figures, 5

The number of references, 40

The number of words in the Abstract, 249

The number of words in the Introduction, 689

The number of words in the Discussion,1292

Abbreviations

ADR, Adriamycin. AHCY, adenosyl-homocysteinase. BHMT, betaine homocysteine methyltransferase. CBS, cystathionine β-synthase. CTH, cystathionine γ-lyase. GCL, glutamate-cysteine ligase. GPX1, glutathione peroxidase. GS, glutathione synthetase. GSH, Glutathione. GSR, glutathione reductase. MAT2A, methionine adenosyltransferase. MTR, 5-methyltetrahydrofolate-homocysteine methyltransferase. MTs, methyltransferases. PTX, Paclitaxel. ROS, reactive oxygen species. SAM, S-Adenosylmethionine. SAH, S-adenosylhomocysteine. STAT3, signal transducer and activator of transcription-3. SLC7A11,

DMD Fast Forward. Published on August 30, 2021 as DOI: 10.1124/dmd.121.000571
This article has not been copyedited and formatted. The final version may differ from this version.

cystine/glutamate antiporter solute carrier family 7 member 11(also known as xCT).

Abstract

Drug resistance of cancer cells is associated with redox homeostasis. The mechanism of acquired resistance of cancer cells to antitumor drugs is not well understood. Our previous studies revealed that drug resistance and highly expressed P-glycoprotein(P-gp) of MCF-7 breast cancer cells was dependent on intracellular redox homeostasis and declined capacity for scavenging reactive oxygen species (ROS). Recently, we observed that, unlike non-tumorigenic cells MCF-10A, three tumorigenic breast cancer cells (MCF-7S, BT474, MDA-MB-231) reprogrammed their metabolism, highly expressed cystathionine-γ-lyase (CTH), and acquired a particular specialty to utilize methionine (Met) to synthesize glutathione (GSH) through the transsulfuration pathway. Interestingly, doxorubicin (adriamycin, ADR) further reprogrammed metabolism of MCF-7 cells sensitive to ADR (MCF-7S), induced it to be another MCF-7 cell line resistant to ADR (MCF-7R) with dramatically down-regulated CTH. The two MCF-7 cells showed distinctly different phenotypes in terms of intracellular GSH, ROS levels, expression and activity of P-gp, CTH and drug resistance. We showed that CTH modulation or the methionine supply brought about the interconversion between MCF-7S and MCF-7R. Methionine deprivation or CTH silencing induced a resistant MCF-7R and lowered paclitaxel activity, yet methionine supplementation or CTH overexpression reversed the above effects, induced a sensitive phenotype of MCF-7S and significantly increased the cytotoxicity of paclitaxel both in vitro and in vivo. IL-6/STAT3 initiated CTH expression and

DMD Fast Forward. Published on August 30, 2021 as DOI: 10.1124/dmd.121.000571
This article has not been copyedited and formatted. The final version may differ from this version.

activity, and the effect on the resistant phenotype was exclusively dependent on CTH and ROS. This study suggests that the IL6/STAT3/CTH axis plays a key role in the transformation between sensitive and resistant MCF-7 cells.

Keywords: CTH; Breast cancer cells; MCF-7; Metabolic reprogramming; IL-6/STAT3, Drug resistance

Significance Statement

CTH plays a key role in transformation between the sensitive and resistant phenotypes of MCF-7 cells and is dependent on the IL-6/STAT3 signaling axis. Modulation of transsulfuration pathway on CTH or IL-6/STAT3, or methionine supplementation is beneficial to reverse the resistance of MCF-7 cells, which indicates a clinical translation potential.

Introduction

Metabolic reprogramming in cancer cells has been a hot topic in recent decades, as the rapid proliferation and survival of tumor cells are dependent upon these metabolic changes (Faubert et al., 2020). Rapidly proliferating cancer cells require reprogrammed pathways of energy metabolism and nutrient acquisition (DeBerardinis et al., 2016; Hanahan et al., 2011) to meet three basic needs, e.g., adequate ATP generation and elevated biosynthesis of small molecules and macromolecules (Cairns et al., 2011). The Warburg effect of aerobic glycolysis was first identified as the major metabolic characteristic occurring in tumors (Liberti et al., 2016). In addition to the dysregulation of glucose metabolism, a broad range of metabolic alterations that distinguish cancer from normal cells have been documented, such as the pentose phosphate pathway (PPP), glutaminolysis and lipid metabolism, and nucleic acid and amino acid turnover (Cormerais et al., 2019; Li et al., 2016). Growing numbers of studies have reported that cancer cells exhibit an altered uptake and utilization of specific amino acids, such as the essential amino acids leucine (Otsuki et al., 2017), tryptophan (Opitz et al., 2020),

DMD Fast Forward. Published on August 30, 2021 as DOI: 10.1124/dmd.121.000571
This article has not been copyedited and formatted. The final version may differ from this version.

and methionine (Sanderson et al., 2019), as well as some amino acids that are generally considered nonessential, including glutamine (Hensley et al., 2013), serine (Mattaini et al., 2016), glycine (Jain et al., 2012), arginine (Patil et al., 2016), asparagine (Knott et al., 2018) and cysteine/cystine (Lo et al., 2008). Knowledge of the metabolic properties of various cancer cells greatly benefits our understanding of the individual particularity and general universality of cancers, but the data are still not sufficient to determine a strategy to circumvent these adaptable cells.

Metabolic reprogramming of cancer cells not only contributes to the proliferation of tumor growth but is also involved in the acquired resistance of tumor cells to antitumor drugs (Rahman et al., 2015). Our previous study demonstrated that the metabolic phenotype of wild-type sensitive MCF-7 cells (MCF-7S) is dramatically different from that of the other cell line of MCF-7 cells with resistance to adriamycin (MCF-7R) (Cao et al., 2013). Continuous exposure to low levels of doxorubicin can induce drug resistance and simultaneously reprogram the metabolic phenotype of MCF-7S cells. Doxorubicin can produce a large amount of ROS and reprogram metabolism, such as the PPP, tricarboxylic acid (TCA) cycle, metabolism of amino acids, purines, glycerol, and fatty acids, and synthesis of nucleic acids and GSH via the cystine/glutamate antiporter system xc^- and cystine. Either inhibition of GSH synthesis or ROS alone can efficiently upregulate the expression and activity of P-gp and hence induce multiple drug resistance, while scavenging ROS with NAC efficiently reverses drug resistance induced by elevated ROS. Increasing evidence suggests that ROS not only trigger mutations and promote growth and metastasis, but also that high baseline levels of ROS are recognized as an important factor for inducing drug resistance in cancer cells. To cope with intensive oxidative stress, living cells normally upregulate antioxidant capabilities for their survival, such as by increasing the biosynthesis of the tripeptide antioxidant GSH (Balendiran et al., 2004). MCF-7S cells can utilize cystine to synthesize GSH through the SLC7A11 transporter to maintain the intracellular oxidative balance. However, for MCF-7R cells, uptake and transport of cystine were significantly inhibited, and GSH was rarely

DMD Fast Forward. Published on August 30, 2021 as DOI: 10.1124/dmd.121.000571
This article has not been copyedited and formatted. The final version may differ from this version.

synthesized via cystine. As the other key source material for the synthesis of GSH, the dependence and utilization of methionine have not been evaluated in sensitive and resistant MCF-7 breast cancer cells, and the underlying mechanism of reprogrammed redox metabolism and a gain of drug resistance has not been well studied.

It is well known that the transsulfuration pathway is largely restricted to a few nonneoplastic tissues, such as the liver, pancreas, and kidneys (Stipanuk, 2004). Recently, we observed that, unlike normal breast and most nonhepatic cells, breast cancer cells alter cellular metabolism and acquire a particular specialty to utilize Met to synthesize GSH through the transsulfuration pathway. In addition, the synthesis enzymes for GSH and the flux through the transsulfuration pathway differ in resistant MCF-7 breast cancer cells and wild-type sensitive MCF-7 cells. To investigate the mechanism of GSH synthesis by Met, here we employed a variety of cell lines to compare the gene and protein levels associated with the sulfur transfer pathway in normal breast cells, multiple breast cancer cells, and sensitive and drug-resistant MCF-7 cells. We focused on the key enzymes and genes involved in metabolic processes of the Met utilization pathway, evaluating the modulation effect on the drug resistance of MCF-7 cells. We aimed to elucidate the molecular regulatory mechanism of Met utilization and a way to reverse drug resistance in breast cancer cells.

Materials and methods

Cell culture

Human breast carcinoma cell lines MCF-7 (MCF-7S), MDA-MB-231, BT474, and human mammary epithelial cell lines MCF-10A were purchased from the American Type Culture Collection (Manassas, VA). MCF-7R were provided by the Institute of Hematology and Blood Diseases Hospital (Tianjin, China). Human mammary epithelial cell lines HMEC were purchased

DMD Fast Forward. Published on August 30, 2021 as DOI: 10.1124/dmd.121.000571
This article has not been copyedited and formatted. The final version may differ from this version.

from Cell Applications Inc (San Diego, CA, USA). MCF-7S, MCF-7R, and BT474 cells were cultured in RPMI 1640 medium (Gibco, Carlsbad, CA, USA) supplemented with 10%(v/v) fetal bovine serum (FBS) (Gibco, Carlsbad, CA, USA) and 100 U/mL penicillin and 1 μg/mL streptomycin at 37 °C with 5% CO_2. MCF-10A and HMEC cells were cultured in DMEM/F-12 medium (Gibco, Carlsbad, CA, USA) supplemented with 10%(v/v) FBS (Gibco, Carlsbad, CA, USA) and 100 U/mL penicillin and 1 μg/mL streptomycin at 37 °C with 5% CO_2. MDA-MB-231 were cultured in Leibovitz's L-15 Medium containing 10%(v/v) FBS, 100 U/mL penicillin and 1 μg/mL streptomycin at 37 °C in 100% air. The medium was changed every other day.

Cell viability assays

The sensitivity of the non-transfected MCF-7 cells and transfected MCF-7 cells to PTX was determined. Cells were seeded into 96-well plates (5×10^3 cells/well) and incubated with the medium containing PTX in different concentrations for 24 h(n=6). A total of 10 μL of cell counting kit-8 (CCK-8) reagent (Beyotime Institute of Biotechnology, China) was added to each well, and plates were incubated for 4 hours at 37°C. Then, the absorbance at 450 nm was measured using fluorescence.

Quantitative real-time polymerase chain reaction (qRT-PCR)

Total cells/tissues RNA was extracted from cells by Trizol reagent (Invitrogen, USA) according to the manufacturer's recommendation and was quantified with ultraviolet spectrophotometry by the standard of OD260/OD280 ratio of 1.6-2.0. Complementary DNA was synthesized with the PrimeScript RT Reagent Kit (Takara Bio, Japan). Quantitative real-time PCR was performed in a CFX96 real-time RT-PCR detection system (Bio-Rad, USA) using SYBR Premix Ex Taq (Takara Bio, Japan) according to the manufacturer's instructions. The primer Sequences used in this study

DMD Fast Forward. Published on August 30, 2021 as DOI: 10.1124/dmd.121.000571
This article has not been copyedited and formatted. The final version may differ from this version.

are listed in Supplementary Table 1. All of the samples were quantified using the comparative Ct method for the relative quantification of gene expression, normalized to the expression of the reference gene actin.

Western blotting analysis

Approximately 50-60 μg of total protein was separated by 10% SDS-PAGE, and transferred to polyvinylidene fluoride membranes (Bio-Rad, Hercules, CA, USA). After blocking with 5% non-fat milk, the membrane was incubated with the Rabbit Monoclonal to CTH (1:1 000, Cell Signaling Technology, USA, 30068), Rabbit monoclonal [EPR10364-57] to P-Glycoprotein (1:1 000, Abcam, USA, ab170904), Mouse monoclonal[9D8] to STAT3 (1:1 000, Abcam, USA, ab119352), Rabbit polyclonal to STAT3(phosphor S727) (1:1 000; Abcam, USA, ab86430,), Rabbit monoclonal [EP2147Y] to STAT3 (phospho Y705) (1:1 000, Abcam, USA, ab76315), GAPDH polyclonal antibody (1:5 000, Bioworld Technology, Inc. , AP0063) overnight at 4 °C, followed by incubation with the HRP-conjugated secondary antibodies for 1 h at 37 °C. The signals were detected with an enhanced chemiluminescence kit (Thermo Fisher Scientific, Waltham, MA, USA) and captured using a ChemiDoc^{TM} XRS+ System (Bio-Rad, Hercules, CA, USA). The intensity of bands was quantified by Image Lab statistical software (Bio-Rad Laboratories, Hercules, CA, USA).

Intracellular ROS and glutathione Measurement.

The intracellular ROS was determined with 2′,7′-dichlorodihydrofluorescein diacetate (DCFH-DA, Beyotime Institute of Biotechnology, China). Cells were incubated with 10μM DCFH-DA at 37 °C for 45 min, then added NaOH: methanol (v: v=1:1) solution and centrifuged at 6000 rpm for 5 min. The supernatant was collected for determination using a Synergy-H1 multi-mode

DMD Fast Forward. Published on August 30, 2021 as DOI: 10.1124/dmd.121.000571
This article has not been copyedited and formatted. The final version may differ from this version.

microplate reader (Bio-Tek Instruments, Inc., USA) at wavelength of 488/535 nm. Intracellular GSH and GSSG were measured using commercially available GSH and GSSG Test Kit (Beyotime Institute of Biotechnology, China) according to the manufacturer's instructions. The ROS, GSH, and GSSG values were normalized to the protein levels, which were measured by BCA protein assay kit (Beyotime Institute of Biotechnology, China).

Nutrient deprivation and supplement

Cells were cultured in the identical medium (RPMI 1640) for at least 3 passages. After washed twice with PBS, cells were received varying concentrations of methionine (Sigma-Aldrich, M9625) using DMEM medium (lacking glutamine, methionine, cystine but containing all other amino acids), with 63.0mg/L L-Cystine dihydrochloride (Sigma-Aldrich, G6727) and 584mg/L L-glutamine (Sigma-Aldrich, G8540) added back in each experiment.

Metabolic tracing

For serine labeling experiments, cells were cultured in the identical medium (RPMI 1640) for at least 3 passages. After washed twice with PBS, cells were cultured in MEM medium (lacking glycine, serine but containing all other amino acids) supplemented with 30mg/L glycine (Sigma-Aldrich, G7126) and 42mg/L [U-^{13}C]-Serine (Shanghai ZZBIO, China) instead of unlabeled serine. The labeling medium was replaced 2 h before cell harvest.

LC-Q/TOF-MS-based metabolite analysis

Metabolites were analyzed using an LC-30A Shimadzu LC system (Kyoto, Japan) coupled to a hybrid quadrupole time-of-flight tandem mass spectrometer (SCIEX TripleTOF® 5600 LC–Q/TOF-MS, Foster City, CA). An XBridge Amide HPLC column (3.5 μm; 4.6 mm×100 mm; Waters, USA) was used for metabolite separation with a column temperature of 40 °C. The flow

DMD Fast Forward. Published on August 30, 2021 as DOI: 10.1124/dmd.121.000571
This article has not been copyedited and formatted. The final version may differ from this version.

rate was 0.4 ml/min. Mass detection was operated in negative ion modes with the following optimized conditions: The masses were scanned over m/z 50–1,000; ion source gas 1 (gas 1), 33 psi; ion source gas 2 (gas 2), 30 psi; Curtain Gas, 30 psi; source temperature, 500 °C; Ion spray voltage, −4.5 kV; declustering potential (DP), −93 V; collision energy (CE), −10V. The mobile phase consisted of solvent A (5 mM ammonium acetate buffer, pH=9, 5% acetonitrile) and solvent B (acetonitrile). The gradient was set as follows: 0–3 min 85% B, 3–6 min 85–30% B, 6–15 min 30–2% B, 15–18 min 2% B, 18–19 min 2–85% B, 19–26 min 85% B. The accurate mass was calibrated by Calibration Delivery System (CDS, AB SCIEX), and automatic calibration was performed every six samples. Peak areas from the total ion current for each metabolite were integrated using MultiQuant v2.0 software (AB/SCIEX). For ^{13}C-labeled experiments, percentage of total GSH pool can be obtained by dividing the peak area of each isotopologue by the summed intensities of all the detected isotopomers.

Transient CTH/STAT3 siRNA transfection

Cells were plated in six-well plates and transfected with Human CTH siRNA (sc-78973, Santa Cruz, USA), Human STAT3 siRNA (sc-29493, Santa Cruz, USA), and Control siRNA (sc-37007, Santa Cruz, USA) using the Lipofectamine® RNAiMAX Transfection Reagent (13778150, Life Technologies, USA) and the Gibco™ Opti-MEM™ I Reduced Serum Media (31985-070, Life Technologies, USA) according to the manufacturer's instructions. After incubation for 48-72 hours, expressions of CTH or STAT3 was monitored by Western blot analysis to confirm the efficiency of the siRNA knockdown.

Lentiviral infection, plasmid transfection and establishment of stable cell lines

Knockdown of CTH in MCF-7S cells with short hairpin RNA (shRNA) or over-expression of

DMD Fast Forward. Published on August 30, 2021 as DOI: 10.1124/dmd.121.000571
This article has not been copyedited and formatted. The final version may differ from this version.

CTH in MCF-7R cells with plasmid, were conducted by Viral Therapy Technologies (Wuhan, China) using lentiviral particles.

For MCF-7S cells, a set of two CTH shRNAs was packed into each viral particle. Cells were selected with 1 μg/mL puromycin until resistant colonies could be identified and propagated. MCF-7S cells that survived puromycin selection after transfection with CTH shRNA or scrambled control shRNA were regarded as shCTH-MCF-7S and shCtrl-MCF-7S, respectively.

CTH shRNA1:

CCGGGCCCAGTTCCTGGAATCTAATCTCGAGATTAGATTCCAGGAACTGGGCTTTTTG

CTH shRNA2:

CCGGGCACCTCATTATCTTTCATAACTCGAGTTATGAAAGATAATGAGGTGCTTTTTG

For MCF-7 cells, over-expressed CTH plasmid was packed into each viral particle. Cells were also selected with 1 μg/mL puromycin. MCF-7 cells that survived puromycin selection after transfection with CTH plasmid or empty vector were regarded as oxCTH-MCF-7 and EV-MCF-7, respectively.

Western blot was used to confirm the efficiency of CTH transfection.

Enzyme-Linked Immunosorbent Assay (ELISA) for IL-6, IL-10

Cells were cultured in 6-well plates with RPMI 1640 containing 10% FBS for 24 h. Then the medium was completely replaced to serum-free medium with or without PTX for another 24 h, and the level of IL-6, IL-10 in supernatant was tested using Human Enzyme-linked immunosorbent assay (ELISA) kit (ExCell Biotech Co., Ltd) according to the manufacturer's instructions. The absorbance was read at 450 nm.

Intracellular accumulation of Rhodamine 123 (Rho 123) Assay

DMD Fast Forward. Published on August 30, 2021 as DOI: 10.1124/dmd.121.000571
This article has not been copyedited and formatted. The final version may differ from this version.

After treatment, cells were incubated with Hank's Balanced Salt Solution (HBSS; 37 °C, pH 7.4) containing 5μM Rho123 (Sigma-Aldrich, R8004) for 2 h. After rinsed the cells with ice-cold HBSS, the cells were lysed and the protein concentrations were measured via the Bradford method using the BCA protein assay kit (Beyotime Institute of Biotechnology, China), the intracellular accumulation of Rho123 was detected by fluorescence microscopy in parallel.

Xenograft studies

Healthy specific-pathogen-free (SPF) female BALB/c-nu/nu mice (20±2 g and 8–10 weeks old) were purchased from the Animal Center of Nanjing Medical University. The experimental procedures were conducted strictly according to the guidelines of the Committee on the Care and Use of Laboratory Animals and the related ethical regulations of China Pharmaceutical University. 6×10^6 exponentially growing MCF-7R cells, MCF-7S-shCtrl cells and MCF-7S-shCTH cells were collected and suspended in 0.2 ml of 1:1 PBS/Matrigel (BD, USA) and then injected into the left flanks of each mice, and estrogen pellets were implanted before injection. When the tumours grown to100 mm^3 (four mice per group), the mice were randomly divided into groups, followed by antitumor treatment.

Mice bearing MCF-7R subcutaneous tumors in their right flank regions were randomly assigned to four groups (4 and 6 mice per group, respectively): 1) control group (saline, i.p.), 2) PTX (5mg/kg/three days, i.p.), 3) methionine (120 mg/kg/day, i.p.) and 4) PTX (5mg/kg/three days, i.p.) + methionine (120 mg/kg/day, i.p.). Mice bearing MCF-7S-shCont and MCF-7S-shCTH subcutaneous tumors in their right flank regions were randomly assigned to six groups (4and 6 mice per group, respectively): 1) control group (saline, i.p.), 2) NAC (1.5 g/L/week added in drinking water), 3) methionine (120

DMD Fast Forward. Published on August 30, 2021 as DOI: 10.1124/dmd.121.000571
This article has not been copyedited and formatted. The final version may differ from this version.

mg/kg/day, i.p.), 4) PTX (5mg/kg/three days, i.p.), 5) PTX (5mg/kg/three days, i.p.) + NAC (1.5 g/L/week added in drinking water) and 6) PTX (5mg/kg/three days, i.p.) + methionine (120 mg/kg/day, i.p.). The longest and shortest diameters of the tumors were measured using a digital caliper twice weekly. At the end of the experiment, all mice were sacrificed by cervical dislocation, and tumours were collected.

Statistical analysis

All of the data were presented as the means ± SD. Statistical comparison between two groups was performed using Student's t test. All statistical analyses were performed with GraphPad Prism 8(GraphPad Software Inc., San Diego, CA). P values less than 0.05 were considered statistically significant (*$p < 0.05$).

Results

MCF-7S cells highly expressed CTH to synthesize GSH via methionine; MCF-7R cells poorly expressed CTH and utilize a small amount of methionine to synthesize GSH

Cystathionine-β-synthase (CBS) and CTH are the key enzymes in the transsulfuration pathway for GSH synthesis (Sbodio et al., 2019). RT-PCR assays revealed that the three

DMD Fast Forward. Published on August 30, 2021 as DOI: 10.1124/dmd.121.000571
This article has not been copyedited and formatted. The final version may differ from this version.

tumorigenic breast cancer cell lines (MCF-7S, BT474, MDA-MB-231) expressed higher CBS and CTH than nontumorigenic cell lines (MCF-10A, HMEC) (Figure 1A and Supplementary Fig. 1A), with much higher expression of CTH in three tumor cells, which was confirmed by Western blotting (Figure 1B). To determine the role of CTH, it was silenced in both breast cancer cells and MCF-10A (Supplementary Fig. 1B) cells. The data showed that CTH siRNA markedly increased intracellular ROS levels in MCF-7S cells, yet it showed little elevation of ROS in MCF-10A cells (Supplementary Fig. 1C). Met deprivation and supplementation disturbed the redox balance in MCF-7S cells, but no obvious disturbance was observed in MCF-10A cells. Moreover, Met deprivation significantly inhibited the growth of three breast cancer cell lines in a time-dependent manner and showed a marginal effect on MCF-10A cells (Supplementary Fig. 1D). These results suggested that unlike nontumorigenic breast cells, tumorigenic breast cancer cells acquired a particular specialty to synthesize GSH by utilizing Met via the transsulfuration pathway and highly expressed CTH.

Our previous study has shown that sensitive MCF-7S and resistant MCF-7R cells possess varied capacities to utilize cystine to synthesize GSH (Ge et al., 2017). RT-PCR examination of CBS and CTH showed that the two cell lines had dramatically different expression levels of CTH, with approximately 7 times higher levels in sensitive than resistant cells (Figure 1C). However, the CBS levels were comparable in MCF-7S and MCF-7R cells both in vitro and in vivo (Figure 1C). Metabolomic analysis of the endogenous metabolites revealed a resistant phenotype of metabolism, with an increase in Met, cystathionine, glutamate and homocysteine levels and a decrease in cysteine and cystine in MCF-7R cells (Figure 1D), indicating reduced utilization of Met and the transsulfuration pathway in MCF-7R cells.

DMD Fast Forward. Published on August 30, 2021 as DOI: 10.1124/dmd.121.000571
This article has not been copyedited and formatted. The final version may differ from this version.

Metabolic flow analysis with [U-^{13}C]-serine showed that serine carbon was incorporated into the GSH pool through transsulfuration-derived cysteine, where there was much higher [M+5] GSH in MCF-7S than in MCF-7R cells (Supplementary Fig. 1E). This result indicated that MCF-7S cells utilized more serine and Met in the synthesis of cystathionine and GSH than MCF-7R cells via the transsulfuration pathway (Supplementary Fig. 1F). The above results strongly suggested that MCF-7S cells tended to optimally utilize Met and highly expressed CTH, while the resistant MCF-7R cells reprogrammed redox stasis by downregulating CTH and use of Met.

Met deprivation induces a change from sensitive phenotypes of MCF-7S cells into resistant MCF-7R cells; Met supplementation reverses the sensitive phenotypes of resistant MCF-7R cells into sensitive MCF-7S cells in vitro and in vivo

In previous studies, it has been demonstrated that a high level of ROS generation in MCF-7 cells induces drug resistance, while scavenging ROS reverses resistance and enhances drug sensitivity(Ge, Cao, Feng, Zhou, Zhang, Yang, Feng, Wang and Aa, 2017). The regulatory effects of Met metabolism on drug sensitivity or resistance were examined. We showed that Met deprivation induced a resistant phenotype of MCF-7 cells, with a significant decrease in the GSH/GSSG ratio (Figure 2A) and an increase in ROS production (Figure 2B) and P-gp expression (Figure 2C). Met supplementation showed the opposite effects and modified the resistant phenotype of MCF-7R cells into a sensitive phenotype. Western blotting showed that supplementary Met significantly downregulated P-gp protein expression in a dose-dependent manner (Figure 2D). The addition of NAC, an efficient ROS scavenger, depressed the high

DMD Fast Forward. Published on August 30, 2021 as DOI: 10.1124/dmd.121.000571
This article has not been copyedited and formatted. The final version may differ from this version.

ROS level (Supplementary Fig. 2A), reduced the expression of P-gp (Figure 2E), and significantly enhanced the intracellular fluorescence intensity of Rho-123 (Figure 2G). In combination with Met supplementation, when MCF-7R cells were exposed to various concentrations of H_2O_2 ranging from 0.5 to 2.0 mM, ROS and P-gp levels correspondingly increased (Figure 2F and Supplementary Fig. 2B) and reversed the function of P-gp, as shown by fluorescence microscopy analysis (Figure 2H). The results of the cell viability analysis at different concentrations of paclitaxel (PTX) showed that compared with the normal control group, Met deprivation promoted cell viability, while the additional Met inhibited cell viability (Supplementary Fig. 2C).

Moreover, the effect of Met on sensitizing antitumor drugs of breast cancer was evaluated in a nude mouse xenograft model of MCF-7R cells. The data showed that although PTX administration markedly decreased GSH levels (Supplementary Fig. 2D) and promoted ROS levels (Supplementary Fig. 2E) and the expression of P-gp in tumor tissues (Supplementary Fig. 2F), simultaneous administration of Met evidently reconstructed the redox balance, reduced ROS and the expression of P-gp, and enhanced the antitumor activity of PTX in terms of reducing the tumor volume relative to that with only PTX (Supplementary Fig. 2G). These results confirmed that supplementary Met had potential effects on reversing drug resistance and enhancing PTX efficacy.

CTH silencing alters the sensitive phenotype of MCF-7S cells to the resistant phenotype of MCF-7R cells; overexpression of CTH modifies the resistant phenotype of MCF-7R cells to the sensitive phenotype of MCF-7S cells. Both effects are dependent on the ROS level.

In addition to the varied sensitivity or resistance to antitumor drugs, MCF-7S and MCF-7R

DMD Fast Forward. Published on August 30, 2021 as DOI: 10.1124/dmd.121.000571
This article has not been copyedited and formatted. The final version may differ from this version.

cells also showed dramatic variation in CTH at both the expression and functional levels. To check the dependence of drug sensitivity or resistance on CTH, CTH was modulated either by transfection with small interfering RNA (siRNA) or lentiviral vector to down- or upregulate CTH expression in MCF-7S and MCF-7R cells (Supplementary Fig. 3A and B). The results showed that CTH silencing transfection induced a resistant phenotype, e.g., the GSH/GSSG ratio was decreased and the ROS level was increased compared with the control group (Figure 3A and B), and the expression of P-gp was remarkably upregulated at both the mRNA and protein levels (Figure 3C). Scavenging of ROS with NAC efficiently lowered ROS and P-gp levels and function in CTH-silenced MCF-7S cells (Supplementary Fig. 3C; Figure 3D and I), strongly suggesting that ROS and P-gp were dependent on CTH modulation and that ROS played a key role in inducing P-gp expression and activity. Conversely, CTH overexpression showed the opposite effect to silencing, gradually turning the resistant phenotype into a sensitive phenotype, i.e., CTH overexpression promoted the GSH/GSSG ratio (Figure 3E), reduced ROS (Figure 3F), and downregulated P-gp at both the mRNA and protein levels (Figure 3G). However, in MCF-7R cells, the overexpression effect of CTH on P-gp expression could be offset by the addition of H_2O_2, an ROS generator, consistent with the functional examination with fluorescence microscopy analysis of the efflux of intracellular Rho123 (Figure 3H and J; Supplementary Fig. 3D). Moreover, PTX cytotoxicity was significantly reduced in cells transfected with CTH-siRNA relative to nontransfected cells (Supplementary Fig. 3E), and CTH-overexpressing cells became more sensitive to PTX (Supplementary Fig. 3F). Overall, the results indicated that P-gp expression and drug sensitivity/resistance of MCF-7 cells were dependent on CTH, which regulated redox homeostasis.

Activation of the IL6/STAT3 axis downregulates CTH and induces a resistant phenotype of MCF-7R cells; silencing of STAT3 upregulates CTH and forms a

DMD Fast Forward. Published on August 30, 2021 as DOI: 10.1124/dmd.121.000571
This article has not been copyedited and formatted. The final version may differ from this version.

sensitive phenotype of MCF-7S cells.

It has been documented that signal transducer and activator of transcription-3 (STAT3) is overexpressed and constitutively activated in breast cancer cells(Qin et al., 2019), and abnormal activity of IL-6/STAT3 relates to stemness maintenance and drug resistance of breast cancer (Huang et al., 2016). The level of STAT3 was therefore assessed in nonresistant MCF-7S cells and resistant MCF-7R cells. As indicated in Figure 4A, total STAT3 protein and tyrosine phosphorylated STAT3 (Tyr^{705}) protein expression was significantly higher in the MCF-7R group than the MCF-7S group. Examination of the upstream regulatory factors of STAT3 revealed that the mRNA expression of both IL-6 and IL-10 increased in MCF-7R cells, but only the secretion levels of the inflammatory factor IL-6 in MCF-7R cells were much higher than those in MCF-7S cells (Figure 4C). After stimulation with IL-6 and IL-10, we showed that IL-6 fully promoted STAT3 activation through the phosphorylation site Tyr^{705} in a dose-dependent manner, whereas IL-10 failed to activate STAT3 (Figure 4B). Moreover, treatment with increased concentrations of PTX in breast cancer cells enhanced IL-6 expression, and subsequently, tyrosine 705 phosphorylation of STAT3 was attenuated (Figure 4A). We also observed that tyrosine phosphorylation (Tyr^{705}) of STAT3 was accompanied by decreased expression of CTH in a dose-dependent manner when treated with IL-6, which suggested that STAT3 was negatively related to CTH expression (Figure 4B). This relationship of $pTyr^{705}$ STAT3 and CTH was observed in MCF-7S and MCF-7R cells treated with different doses of PTX, indicating that IL-6/$pTyr^{705}$ STAT3 and CTH conferred resistance to PTX treatment (Figure 4A).

Moreover, we observed that IL-6 could reduce the GSH/GSSG ratio (Supplementary Fig. 4A), elevate the ROS level (Figure 4D), significantly downregulate CTH expression and upregulate P-gp expression (Figure 4E), and finally reduce the antitumor activity of PTX (Supplementary Fig. 4B). In contrast to the effect of IL6/STAT3 activation, the presence of NAC inhibited the upregulation of P-gp, indicating that IL6/STAT3-induced high P-gp expression was ROS-dependent. Consistently, the cytotoxic effect of PTX was significantly higher when treated with a combination of IL-6 and NAC than when treated with IL-6 alone

DMD Fast Forward. Published on August 30, 2021 as DOI: 10.1124/dmd.121.000571
This article has not been copyedited and formatted. The final version may differ from this version.

(Figure 4F). Conversely, STAT3 silencing in MCF-7R cells showed an effect completely opposite to that of STAT3 phosphorylation activation. In detail, efficient silencing of STAT3 induced a sensitive phenotype in MCF-7 cells, e.g., a significantly increased GSH/GSSG ratio (Supplementary Fig. 4C) and CTH expression (Figure 4G), but reduced ROS levels (Figure 4F) and P-gp expression (Figure 4G). H_2O_2 treatment effectively reversed the effects induced by STAT3 silencing, such as elevated P-gp expression and weakened antitumor potency (Figure 4G; Supplementary Fig. 4D). It was suggested that the effect of STAT3 was dependent on ROS levels. Interestingly, we showed that the expression of $pTyr^{705}$ STAT3 was enhanced by H_2O_2 (Figure 4G), as treatment with NAC and H_2O_2 decreased and increased IL-6 expression (Supplementary Fig. 4E).

The effect of the IL6/STAT3 axis on both the sensitivity and resistance of MCF-7 cells is dependent on CTH

The role of CTH was further probed to elucidate the mechanism bridging IL6/STAT3 and intracellular redox homeostasis and P-gp levels. Strikingly, CTH overexpression substantially rescued the resistant phenotype of decreased GSH (Supplementary Fig. 4F), increased ROS levels (Figure 5A) and the expression of P-gp (Figure 5B), as well as drug resistance, which was induced by STAT3 activation (Figure 5C). Conversely, silence of CTH successfully deactivated these effects induced by STAT3 silencing (Supplementary Fig. 4G; Figure 5D-F). These data suggested that CTH was a key factor bridging IL6/STAT3 and the sensitive or resistant phenotype of MCF-7 cells.

In vivo modulation of Met and CTH alters the drug resistance of breast cancer cells in nude mouse xenografts

We further established nude mouse xenograft models using MCF-7S cells stably transduced with either nontargeting shRNA control (sh-Ctrl) or sh-CTH. In MCF-7S-sh-Ctrl xenograft mouse tumor tissue samples, either supplementary NAC or Met combined with PTX

DMD Fast Forward. Published on August 30, 2021 as DOI: 10.1124/dmd.121.000571
This article has not been copyedited and formatted. The final version may differ from this version.

increased GSH levels (Supplementary Fig. 5A), depressed ROS levels (Figure 6A), downregulated P-gp expression (Figure 6B), and inhibited tumor growth with lower tumor weights after two weeks of treatment compared with the PTX group (Figure 6C), indicating that GSH promotion was responsible for the enhanced effect of PTX. Moreover, PTX clearly elevated $pTyr^{705}$STAT3 in both MCF-7S-sh-Ctrl and MCF-7S-sh-CTH xenografts, while NAC and Met had little effect on $pTyr^{705}$STAT3 (Figure 6B and E).

In CTH-silenced mouse tumor tissue samples, PTX treatment significantly reduced GSH (Supplementary Fig. 5B), increased ROS (Figure 6D), upregulated the expression of P-gp (Figure 6E), and showed a marginal effect on tumor growth. NAC supplementation efficiently reconstructed the redox balance perturbed by PTX (Figure 6D and E), downregulated the expression of P-gp (Figure 6E), and reversed PTX resistance (Figure 6F). Met supplementation did not show the same effect as NAC (Figure 6D-F), suggesting that silencing of CTH was responsible for the disappearance of the drug resistance reversal effect. Together with the effect of Met on sensitizing PTX in a nude mouse xenograft model of MCF-7R cells, the above data indicated that CTH played a key role in the resistant or sensitive phenotype of MCF-7 cells in vitro and in vivo. Consistent with the in vitro results, compared with MCF-7S-sh-Ctrl xenograft models, MCF-7S-sh-CTH xenograft models were less sensitive to PTX.

Discussion

1. Breast cancer cells are characterized by high expression and activity of CTH and enhanced utilization of methionine for GSH synthesis

The transsulfuration pathway plays a central role in the maintenance of intracellular redox homeostasis. It has been estimated that approximately 50% of cysteine in GSH is derived from methionine via transsulfuration in hepatic cells (McBean, 2012). However, transsulfuration is confined to the liver and is either absent or present at very low levels outside of the liver

DMD Fast Forward. Published on August 30, 2021 as DOI: 10.1124/dmd.121.000571
This article has not been copyedited and formatted. The final version may differ from this version.

(Finkelstein, 1990; Stipanuk, 2004). Typically, the transsulfuration pathway is inactive, the expression of CBS and CTH is minimized, and hence little Met is required for normal breast cells, as well as breast tissues (Sen et al., 2015). Surprisingly, we observed that three breast cancer cells altered their metabolism and acquired the capacity to synthesize GSH via the transsulfuration pathway. Much higher expression of CTH was observed in the three breast cancer cell lines, i.e., MCF-7S, BT474, MDA-MB-231, than in normal MCF-10A cells. Indeed, cancer cells experience higher oxidative stress from ROS than their normal counterparts, and as a result, maintenance of the antioxidant GSH is essential for the survival and proliferation of cancer cells (Bansal et al., 2018).

Cystine and methionine are the two primary source materials for the synthesis of GSH. Our previous study showed that MCF-7S and MCF-7R cells have a varied dependence on cystine and significantly different expression of SLC7A11, the transporter for the influx of cystine. Downregulated SLC7A11 greatly restricts cystine uptake and reduces GSH biosynthesis in MCF-7R cells (Ge, Cao, Feng, Zhou, Zhang, Yang, Feng, Wang and Aa, 2017). In the present study, our data showed that wild-type MCF-7 cells and BT474 and MDA-MB-231 cells were heavily dependent on Met. Met deprivation alone greatly inhibited the viability of breast cancer cell lines, indicating the dependence of cancer cells on Met, which contributed to the antioxidation ability. Consistently, unlike most normal, nonhepatic, nontumorigenic cells, the property of ‘methionine dependency’ has also been documented for multiple malignant cell lines, e.g., breast, bladder, colon, glioma, kidney, melanoma, and prostate cancer (Halpern et al., 1974; Mecham et al., 1983). Additionally, we observed that without methionine, the viability of breast cancer cells became weak in the presence of cysteine, indicating that exogenous cysteine alone was far from sufficient for GSH synthesis and cell survival. This finding is also in agreement with a previous report showing that cancer cells of the prostate require the methionine and transsulfuration pathways to support proliferation (Zhu et al., 2019). Our results showed that breast cancer cells preferentially consumed Met as the source material to synthesize cystathionine and GSH via the transsulfuration pathway, which is consistent with Borrego’s findings (Borrego et al., 2016). The proliferation and survival of

DMD Fast Forward. Published on August 30, 2021 as DOI: 10.1124/dmd.121.000571
This article has not been copyedited and formatted. The final version may differ from this version.

MCF-7 cells were heavily dependent on CTH and Met utilization.

2. The interconversion between the sensitive and resistant phenotypes of breast cancer cells is dependent on Met and CTH

Relative to normal breast cells, metabolic reprogramming takes place in three breast cancer cells, including wild-type MCF-7S cells, which are characterized by highly expressed CTH and becoming dependent on Met. Interestingly, relative to MCF-7S, metabolic reprogramming occurs again in resistant MCF-7R cells, and these cells express rather low CTH and are hardly dependent on Met. In fact, the baseline level of CTH in resistant MCF-7R cells was only 1/7 of that in sensitive MCF-7S cells, indicating lower antioxidative ability. Consistently, the basal level of intracellular Met was significantly higher in MCF-7R cells than in MCF-7S cells due to a reduced capacity to utilize Met in MCF-7R than in MCF-7S cells, mediated by CTH (Hecht et al., 2016; Wang et al., 2004); hence, the ROS level was higher in MCF-7R.

To our surprise, deprivation or excessive supplementary Met had distinctly different effects on MCF-7 cells, and CTH modulated the interconversion between the sensitive phenotype of MCF-7S and the resistant phenotype of MCF-7R cells. In detail, although the sensitive phenotype of MCF-7S cells expressed much CTH, Met deprivation still modified the sensitive phenotype of MCF-7S cells into a resistant phenotype of MCF-7R, with a significantly reduced GSH/GSSG ratio, increased intracellular ROS, upregulated P-gp expression and activity, and decreased PTX cytotoxicity. However, Met supplementation reversed the above effects as long as the resistant phenotype of MCF-7R cells expressed a small amount of CTH, modifying the resistant phenotype of MCF-7R cells into a sensitive phenotype of MCF-7S cells, similar to the effect of the ROS scavenger N-acetylcysteine (NAC), and it significantly increased the cytotoxicity of paclitaxel. Conversely, the effect of supplementary methionine disappeared in CTH-silenced MCF-7 cells both in vitro and in vivo, suggesting the key importance of CTH. Moreover, CTH silencing or overexpression showed similar effects to Met deprivation or supplementation. Thus, CTH silencing turned the sensitive phenotype of

DMD Fast Forward. Published on August 30, 2021 as DOI: 10.1124/dmd.121.000571
This article has not been copyedited and formatted. The final version may differ from this version.

MCF-7S cells into resistant MCF-7R cells, and CTH overexpression facilitated the modification of the resistant phenotype of MCF-7R cells into MCF-7S cells. It is strongly suggested that CTH is the key enzyme modulating the interconversion between the sensitive and resistant phenotypes of breast cancer cells and that this effect is partially dependent on Met.

3. Regulation of CTH by the IL6/STAT3 axis

As our data suggested that CTH was of crucial importance in determining the sensitive and resistant phenotype of MCF-7 cells, the initial modulation factors were further probed. Our data showed that ADR and PTX significantly increased the first messenger of IL-6 and IL10. According to a previous report, IL-6 commonly activates downstream JAK/STAT signaling pathways in breast cancer models (Banerjee et al., 2016), and both IL-6 and its receptor STAT3 signaling are involved in drug resistance, including breast cancer resistance (Conze et al., 2001; Sonnenblick et al., 2015; Yi et al., 2013). STAT3 could shift noncancer stem cell (non-CSC) dynamics towards CSCs and regulate its downstream genes, leading to resistance in breast cancer cells (Cheng et al., 2018). A comparative study revealed that IL-6 levels and STAT3 phosphorylation at Y705 were significantly higher in MCF-7R than in MCF-7S cells. A further study showed that IL-6 was positively correlated with p-STAT3 Y705 and negatively correlated with CTH in MCF-7 cells. IL-6 efficiently promoted pSTAT3, and activation of the IL-6/STAT3 axis markedly inhibited CTH, induced a resistant phenotype of MCF-7 cells, and finally offset the antitumor activity of PTX. In contrast, silencing of STAT3 markedly increased CTH, reversed the resistant phenotype of MCF-7R cells into a sensitive phenotype of MCF-7S cells, and enhanced the antitumor activity of PTX. The above changes could be reversed by inhibition or knockdown of CTH, suggesting that the effect of STAT3 was dependent on CTH function. It is suggested that the IL-6/STAT3 axis is the primary modulator responsible for the expression and activity of CTH as follows: PTX-IL6-STAT3-CTH-GSH-ROS-P-gp-Drug resistance (Figure Visual abstract).

Limitation

DMD Fast Forward. Published on August 30, 2021 as DOI: 10.1124/dmd.121.000571
This article has not been copyedited and formatted. The final version may differ from this version.

Methionine supplementation or deprivation can be easily controlled in in vitro studies with various cell lines. However, methionine starvation is impossible in animal studies performed for weeks because methionine is contained in food and protein sources. Therefore, it is not possible to examine the effect of methionine deprivation on inducing sensitive MCF-7S cells into resistant MCF-7R cells in vivo. Alternatively, we fed the animals inoculated with resistant MCF-7R cells for two weeks with sufficient methionine, and the results showed that excessive methionine gradually reversed the resistant phenotype of MCF-7R into the sensitive MCF-7S cells. Moreover, precise genetic modification of CTH targeting inoculated tumors was rather difficult and hence not performed in xenograft animals. Alternatively, we showed that the above effects of the methionine supply on MCF-7R cells of the xenograft mice were not observed in the xenograft mice inoculated with silenced CTH cells of MCF-7S, confirming that CTH plays a key role in vivo.

As ROS is a key intermediate in the proposed mechanism modulated by methionine, rigorous measurements are needed. Unfortunately, the probe, DCFH-DA, does not fulfill the criteria. Many publications have previously pointed out the pitfalls and inadequacies of using DCFH-DA probe. For example, this probe does not react with hydrogen peroxide, even though the objective has been to measure hydrogen peroxide. More attention needs to be paid with regard to the nature of the ROS formed in cancer cells in response to methionine modulation(Chen et al., 2010).

Conclusions

Our findings suggest that breast cancer cells reprogram redox metabolism and acquire a particular specialty to synthesize GSH through the transsulfuration pathway. Both in vitro and in vivo studies suggested that CTH played a key role in redox homeostasis and defined the sensitive or resistant phenotype of MCF-7 cells. For the first time, we successfully made interconversion between sensitive MCF-7S and resistant MCF-7R cells either by alteration of CTH or supplementary amount of methionine. CTH upregulation or Met supplementation

DMD Fast Forward. Published on August 30, 2021 as DOI: 10.1124/dmd.121.000571
This article has not been copyedited and formatted. The final version may differ from this version.

showed a similar effect to scavenging ROS and induced a sensitive phenotype of MCF-7 cells, while CTH downregulation or Met depletion had a similar effect to excessive ROS and induced a resistant phenotype. The results indicate that CTH activity and the methionine supply are responsible for the phenotypes and function to transform between resistant and sensitive phenotypes of MCF-7 cells. The IL-6/STAT3 axis dominates the expression and activity of CTH, increases the sensitivity or resistance of MCF-7 cells, and cannot bypass CTH activity.

Acknowledgments and Footnotes

This work was supported by the National Natural Science Foundation of China [81773814, 81803622, 81803624], China Postdoctoral Science Found [2018M640498] and the Jiangsu postdoctoral grant program [2018Z092].

Author's contributions

Participated in research design: Jiye Aa、Honghao Zhou、Guangji Wang、Yuan Xie

Conducted experiments: Zhaoyi Tan、Chun Ge、Chen Xu

Contributed new reagents or analytic tools: Dong Feng、Bei Cao

Performed data analysis: Zhaoyi Tan、Chun Ge

Wrote or contributed to the writing of the manuscript: Jiye Aa、Zhaoyi Tan、Dong Feng

Conflict of Interest

No author has an actual or perceived conflict of interest with the contents of this article.

DMD Fast Forward. Published on August 30, 2021 as DOI: 10.1124/dmd.121.000571
This article has not been copyedited and formatted. The final version may differ from this version.

Reference

Balendiran GK, Dabur R, and Fraser D (2004). The role of glutathione in cancer. *Cell Biochem Funct* 22: 343-352.

Banerjee K, and Resat H (2016). Constitutive activation of STAT3 in breast cancer cells: A review. *Int J Cancer* 138: 2570-2578.

Bansal A, and Simon MC (2018). Glutathione metabolism in cancer progression and treatment resistance. *J Cell Biol* 217: 2291-2298.

Borrego SL, Fahrmann J, Datta R, Stringari C, Grapov D, Zeller M, Chen Y, Wang P, Baldi P, Gratton E, et al. (2016). Metabolic changes associated with methionine stress sensitivity in MDA-MB-468 breast cancer cells. *Cancer Metab* 4: 9.

Cairns RA, Harris IS, and Mak TW (2011). Regulation of cancer cell metabolism. *Nat Rev Cancer* 11: 85-95.

Cao B, Li M, Zha W, Zhao Q, Gu R, Liu L, Shi J, Zhou J, Zhou F, Wu X, et al. (2013). Metabolomic approach to evaluating adriamycin pharmacodynamics and resistance in breast cancer cells. *Metabolomics* 9: 960-973.

Chen X, Zhong Z, Xu Z, Chen L, and Wang Y (2010). 2',7'-Dichlorodihydrofluorescein as a fluorescent probe for reactive oxygen species measurement: Forty years of application and

controversy. *Free Radic Res* 44: 587-604.

Cheng CC, Shi LH, Wang XJ, Wang SX, Wan XQ, Liu SR, Wang YF, Lu Z, Wang LH, and Ding Y (2018). Stat3/Oct-4/c-Myc signal circuit for regulating stemness-mediated doxorubicin resistance of triple-negative breast cancer cells and inhibitory effects of WP1066. *Int J Oncol* 53: 339-348.

Conze D, Weiss L, Regen PS, Bhushan A, Weaver D, Johnson P, and Rincon M (2001). Autocrine production of interleukin 6 causes multidrug resistance in breast cancer cells. *Cancer Res* 61: 8851-8858.

Cormerais Y, Vucetic M, and Pouyssegur J (2019). Targeting amino acids transporters (SLCs) to starve cancer cells to death. *Biochem Biophys Res Commun* 520: 691-693.

DeBerardinis RJ, and Chandel NS (2016). Fundamentals of cancer metabolism. *Sci Adv* 2: e1600200.

Faubert B, Solmonson A, and DeBerardinis RJ (2020). Metabolic reprogramming and cancer progression. *Science* 368: eaaw5473.

Finkelstein JD (1990). Methionine metabolism in mammals. *J Nutr Biochem* 1: 228-237.

Ge C, Cao B, Feng D, Zhou F, Zhang J, Yang N, Feng S, Wang G, and Aa J (2017). The down-regulation of SLC7A11 enhances ROS induced P-gp over-expression and drug resistance in MCF-7 breast cancer cells. *Sci Rep* 7: 3791.

Halpern BC, Clark BR, Hardy DN, Halpern RM, and Smith RA (1974). The effect of replacement of methionine by homocystine on survival of malignant and normal adult mammalian cells in culture. *Proc Natl Acad Sci U S A* 71: 1133-1136.

Hanahan D, and Weinberg RA (2011). Hallmarks of cancer: the next generation. *Cell* 144,

646-674.

Hecht F, Pessoa CF, Gentile LB, Rosenthal D, Carvalho DP, and Fortunato RS (2016). The role of oxidative stress on breast cancer development and therapy. *Tumour Biol* 37: 4281-4291.

Hensley CT, Wasti AT, and DeBerardinis RJ (2013). Glutamine and cancer: cell biology, physiology, and clinical opportunities. *J Clin Invest* 123: 3678-3684.

Huang WC, Hung CM, Wei CT, Chen TM, Chien PH, Pan HL, Lin YM, and Chen YJ (2016). Interleukin-6 expression contributes to lapatinib resistance through maintenance of stemness property in HER2-positive breast cancer cells. *Oncotarget* 7: 62352-62363.

Jain M, Nilsson R, Sharma S, Madhusudhan N, Kitami T, Souza AL, Kafri R, Kirschner MW, Clish CB, and Mootha VK (2012). Metabolite profiling identifies a key role for glycine in rapid cancer cell proliferation. *Science* 336: 1040-1044.

Knott SRV, Wagenblast E, Khan S, Kim SY, Soto M, Wagner M, Turgeon MO, Fish L, Erard N, Gable AL, et al. (2018). Asparagine bioavailability governs metastasis in a model of breast cancer. *Nature* 554: 378-381.

Li Z, and Zhang H (2016). Reprogramming of glucose, fatty acid and amino acid metabolism for cancer progression. *Cell Mol Life Sci* 73: 377-392.

Liberti MV, and Locasale JW (2016). The Warburg Effect: How Does it Benefit Cancer Cells? *Trends Biochem Sci* 41: 211-218.

Lo M, Wang YZ, and Gout PW (2008). The x(c)- cystine/glutamate antiporter: a potential target for therapy of cancer and other diseases. *J Cell Physiol* 215: 593-602.

Mattaini KR, Sullivan MR, and Vander Heiden MG (2016). The importance of serine

metabolism in cancer. *J Cell Biol* 214: 249-257.

McBean GJ (2012). The transsulfuration pathway: a source of cysteine for glutathione in astrocytes. *Amino Acids* 42: 199-205.

Mecham JO, Rowitch D, Wallace CD, Stern PH, and Hoffman RM (1983). The metabolic defect of methionine dependence occurs frequently in human tumor cell lines. *Biochem Biophys Res Commun* 117: 429-434.

Opitz CA, Somarribas Patterson LF, Mohapatra SR, Dewi DL, Sadik A, Platten M, and Trump S (2020). The therapeutic potential of targeting tryptophan catabolism in cancer. *Br J Cancer* 122: 30-44.

Otsuki H, Kimura T, Yamaga T, Kosaka T, Suehiro JI, and Sakurai H (2017). Prostate Cancer Cells in Different Androgen Receptor Status Employ Different Leucine Transporters. *Prostate* 77: 222-233.

Patil MD, Bhaumik J, Babykutty S, Banerjee UC, and Fukumura D (2016). Arginine dependence of tumor cells: targeting a chink in cancer's armor. *Oncogene* 35: 4957-4972.

Qin JJ, Yan L, Zhang J, and Zhang WD (2019). STAT3 as a potential therapeutic target in triple negative breast cancer: a systematic review. *J Exp Clin Cancer Res* 38: 195.

Rahman M, and Hasan MR (2015). Cancer Metabolism and Drug Resistance. *Metabolites* 5: 571-600.

Sanderson SM, Gao X, Dai Z, and Locasale JW (2019). Methionine metabolism in health and cancer: a nexus of diet and precision medicine. *Nat Rev Cancer* 19: 625-637.

Sbodio JI, Snyder SH, and Paul BD (2019). Regulators of the transsulfuration pathway. *Br J Pharmacol* 176: 583-593.

Sen S, Kawahara B, Gupta D, Tsai R, Khachatryan M, Roy-Chowdhuri S, Bose S, Yoon A, Faull K, Farias-Eisner R, et al. (2015). Role of cystathionine beta-synthase in human breast Cancer. *Free Radic Biol Med* 86: 228-238.

Sonnenblick A, Brohee S, Fumagalli D, Vincent D, Venet D, Ignatiadis M, Salgado R, Van den Eynden G, Rothe F, Desmedt C, et al. (2015). Constitutive phosphorylated STAT3-associated gene signature is predictive for trastuzumab resistance in primary HER2-positive breast cancer. *BMC Med* 13: 177.

Stipanuk MH (2004). Sulfur amino acid metabolism: pathways for production and removal of homocysteine and cysteine. *Annu Rev Nutr* 24: 539-577.

Wang J, Huff AM, Spence JD, and Hegele RA (2004). Single nucleotide polymorphism in CTH associated with variation in plasma homocysteine concentration. *Clin Genet* 65: 483-486.

Yi EH, Lee CS, Lee JK, Lee YJ, Shin MK, Cho CH, Kang KW, Lee JW, Han W, Noh DY, et al. (2013). STAT3-RANTES autocrine signaling is essential for tamoxifen resistance in human breast cancer cells. *Mol Cancer Res* 11: 31-42.

Zhu J, Berisa M, Schworer S, Qin W, Cross JR, and Thompson CB (2019). Transsulfuration Activity Can Support Cell Growth upon Extracellular Cysteine Limitation. *Cell Metab* 30: 865-876 e865.

DMD Fast Forward. Published on August 30, 2021 as DOI: 10.1124/dmd.121.000571
This article has not been copyedited and formatted. The final version may differ from this version.

Legends for Figures

Visual abstract

A schematic diagram showing that the IL-6/STAT3-CTH signaling pathway plays a key role in contributing the redox hemostasis in MCF-7S and MCF-7R cells. There is a negative regulation between the IL-6/STAT3 signaling axis and CTH expression and activity. Supplementation with methionine or overexpression of CTH downregulates ROS and P-gp expression and reverses the drug resistance of MCF-7R cells.

Figure 1 The expression and activity of cystathionine-γ-lyase in MCF-7S and MCF-7R cells.

(A) Examination of CTH mRNA, (B) protein expression levels in tumorigenic breast cancer

DMD Fast Forward. Published on August 30, 2021 as DOI: 10.1124/dmd.121.000571
This article has not been copyedited and formatted. The final version may differ from this version.

cell lines (MCF-7S, BT474, MDA-MB-231) and the nontumorigenic cell line (MCF-10A, HMEC) (n=4). (C) Heatmaps of the mRNA expression levels of metabolic enzymes, (D) metabolites involved in methionine and cysteine metabolism. Dark red and dark blue indicate higher and lower abundances of the metabolite, and dark orange and dark green indicate higher and lower expression levels of the genes, respectively(n=4). All data are represented as the mean ± SD. Statistical significance was determined by the Student's t-test. *P < 0.05, * *P < 0.01, * * *P < 0.001 vs. the control group.

Figure 2 Treatment with Met modifies the sensitive and resistant phenotypes of MCF-7 cells.

(A) The cellular GSH/GSSG ratio, (B) ROS levels and (C) P-gp mRNA expression levels were measured in MCF-7 cells cultured in Met-deprived/added medium for 48 h(n=4). (D) P-gp protein levels in MCF-7 cells treated with Met (0, 30, 75, 150 mg/L) for 48 h. GAPDH was used as an internal control. (E) P-gp expression in MCF-7S cells cultured in medium free of Met for 48 h or with 10 mM NAC at 36 h(n=4). (F) P-gp expression in MCF-7R cells cultured in medium with Met (150 mg/L) for 48 h or with H_2O_2 at a series of concentrations as indicated at 24 h(n=4). (G) P-gp function as indicated by intracellular Rho 123 accumulation. Scale bar, 100 μm. (H) The viability of MCF-7 cells treated with PTX with or without Met(n=4). All data are represented as the mean ± SD. Statistical significance was determined by the Student's t-test. *P < 0.05, * *P < 0.01, * * *P < 0.001 vs. the control group.

Figure 3 Transformation of sensitive and resistant phenotypes of MCF-7 cells by CTH modulation.

(A) The cellular GSH/GSSG ratio, (B) ROS levels and (C) P-gp mRNA expression levels were measured in CTH-siRNA MCF-7S cells(n=4). (D) CTH-knockdown MCF-7S cells were treated with NAC (10 mM) for 12 h. P-gp expression was analyzed by RT-PCR(n=4) and

DMD Fast Forward. Published on August 30, 2021 as DOI: 10.1124/dmd.121.000571
This article has not been copyedited and formatted. The final version may differ from this version.

Western blotting. (E) The cellular GSH/GSSG ratio, (F) ROS levels and (G) P-gp expression levels were measured in CTH-overexpressing MCF-7R cells(n=4). (H) CTH-overexpressing MCF-7R cells were treated with 0.5 mM H_2O_2 for 12 h. P-gp expression was analyzed by RT-PCR(n=4) and Western blotting. (I, J) The effect of NAC (10 mM, 12 h) or H_2O_2 (0.5 mM, 12 h) on P-gp function was confirmed by fluorescence microscopy analysis of intracellular Rho123 accumulation in CTH-silenced MCF-7S or CTH-overexpressing MCF-7R cells. Scale bar, 100 μm. All data are represented as the mean ± SD. Statistical significance was determined by the Student's t-test. *P < 0.05, * *P < 0.01, * * *P < 0.001 vs. the control group.

Figure 4 The regulatory effect of the IL-6/STAT3 signaling axis on the resistant phenotype of MCF-7 cells

(A) Expression of pTyr^{705}STAT3, pSer^{727}STAT3, STAT3, CTH and IL-6(n=4) in MCF-7S and MCF-7R cells and in MCF-7S cells (nM) and MCF-7R cells (μM) treated with PTX. (B) The expression of pTyr^{705}STAT3, pSer727STAT3, STAT3, and CTH was examined in MCF-7S cells treated with IL-6 or IL-10 for 24h. (C) IL-6 and IL-10 mRNA levels were determined using real-time PCR. The levels of IL6 and IL-10 in the culture supernatants were examined by ELISA(n=3). (D) ROS levels. MCF-7S cells were treated with NAC (10 mM) for 12 h, and IL-6 (20 ng/ml) for 24 h(n=4). (E) P-gp expression. (F) ROS levels in STAT3-knockdown MCF-7R cells treated with 0.5 mM H_2O_2 for 12 h. (G) P-gp expression(n=4). All data are represented as the mean ± SD. Statistical significance was determined by the Student's t-test. *P < 0.05, * *P < 0.01, * * *P < 0.001 vs. the control group.

Figure 5 The role of CTH in bridging the IL-6/STAT3 signaling axis and drug resistance of MCF-7 cells.

(A) ROS levels. (B) P-gp expression level in CTH-overexpressing MCF-7R cells treated with IL-6 (20 ng/ml) for 24 h(n=4). (C) Cell viability assay in CTH-overexpressing MCF-7R cells

DMD Fast Forward. Published on August 30, 2021 as DOI: 10.1124/dmd.121.000571
This article has not been copyedited and formatted. The final version may differ from this version.

treated with PTX or in combination with IL-6 (20 ng/ml) for 24 h(n=4). (D) ROS levels. (E) P-gp expression levels in MCF-7R cells after STAT3 and CTH were knocked down individually or simultaneously(n=4). (F) Cell viability of MCF-7 cells when STAT3 and CTH were knocked down when treated with PTX for 24 h(n=4). All data are represented as the mean ± SD. Statistical significance was determined by the Student's t-test. *P < 0.05, * *P < 0.01, * * *P < 0.001 vs. the control group.

Figure 6 Met and CTH regulate redox homeostasis and drug resistance of the tumor in nude mouse xenografts inoculated with MCF-7S-sh-Ctrl or MCF-7S-sh-CTH breast cancer cells.

(A) ROS levels and (B) P-gp expression levels were assayed in tumor tissues from the MCF-7S-sh-Ctrl xenograft model(n=4). (C) Xenograft tumors derived from MCF-7S-sh-Ctrl xenograft models (n = 4). Tumor weight. (D) ROS levels and (E) P-gp expression levels were assayed in tumor tissues from the MCF-7S-sh-CTH xenograft model(n=4). (F) Xenograft tumors derived from MCF-7S-sh-CTH xenograft models (n = 4). Tumor weight. All data are represented as the mean ± SD. Statistical significance was determined by the Student's t-test. *P < 0.05, * *P < 0.01, * * *P < 0.001 vs. the control group.

Figure 1

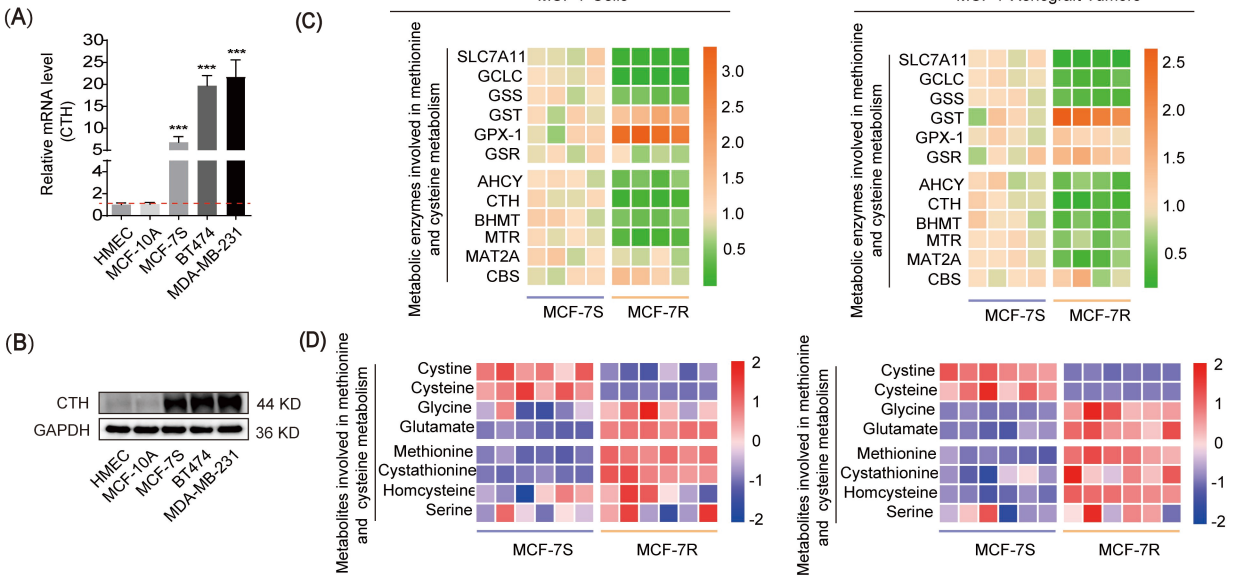
(A)
Relative mRNA level (CTH)
30
25
20
15
10
5
4
2
0
***
***
***
HMEC
MCF-10A
MCF-7S
BT474
MDA-MB-231
(B)
CTH
GAPDH
44 KD
36 KD
HMEC
MCF-10A
MCF-7S
BT474
MDA-MB-231
(C)
MCF-7 Cells
MCF-7 Xenograft Tumors
Metabolic enzymes involved in methionine and cysteine metabolism
SLC7A11
GCLC
GSS
GST
GPX-1
GSR
AHCY
CTH
BHMT
MTR
MAT2A
CBS
3.0
2.5
2.0
1.5
1.0
0.5
2.5
2.0
1.5
1.0
0.5
MCF-7S
MCF-7R
(D)
Metabolites involved in methionine and cysteine metabolism
Cystine
Cysteine
Glycine
Glutamate
Methionine
Cystathionine
Homcysteine
Serine
2
1
0
-1
-2
MCF-7S
MCF-7R

Figure 2

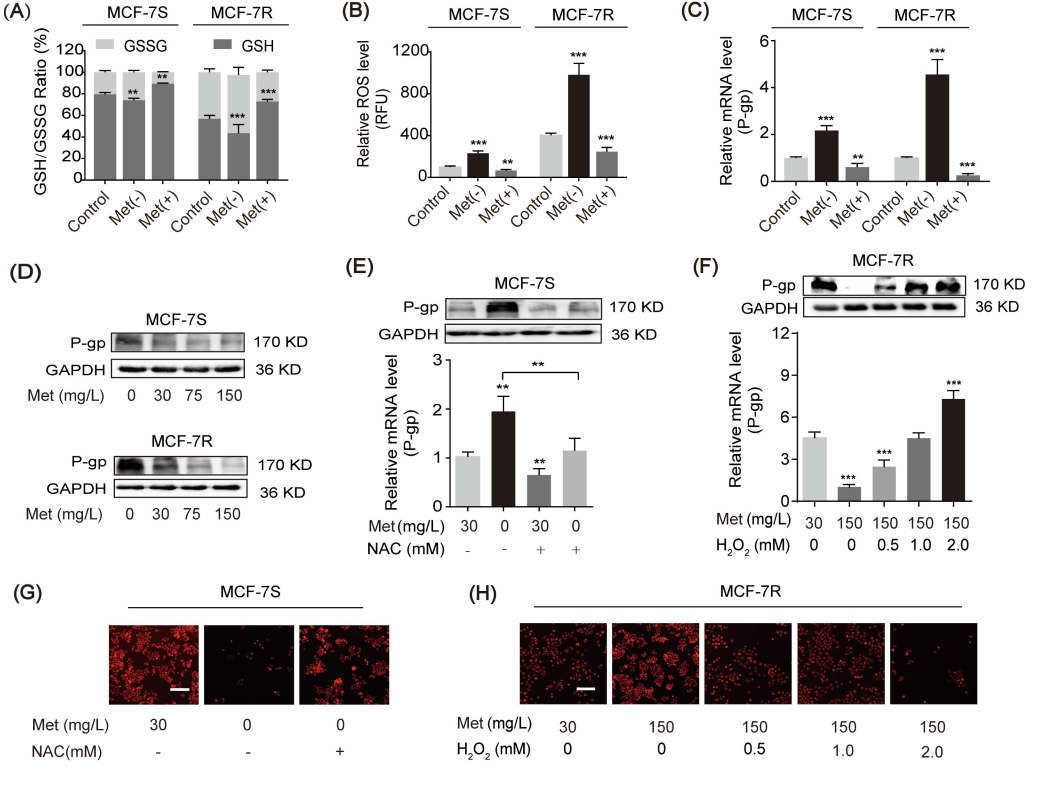
(A)
MCF-7S
MCF-7R
GSSG
GSH
GSH/GSSG Ratio (%)
120
100
80
60
40
20
0
**
***
***
Control
Met(-)
Met(+)
Control
Met(-)
Met(+)
(B)
MCF-7S
MCF-7R
Relative ROS level (RFU)
1200
800
400
0
***
**
***
***
Control
Met(-)
Met(+)
Control
Met(-)
Met(+)
(C)
MCF-7S
MCF-7R
Relative mRNA level (P-gp)
6
4
2
0
***
***
**
***
Control
Met(-)
Met(+)
Control
Met(-)
Met(+)
(D)
MCF-7S
P-gp
170 KD
GAPDH
36 KD
Met (mg/L) 0 30 75 150
MCF-7R
P-gp
170 KD
GAPDH
36 KD
Met (mg/L) 0 30 75 150
(E)
MCF-7S
P-gp
170 KD
GAPDH
36 KD
Relative mRNA level (P-gp)
3
2
1
0
**
**
**
Met (mg/L) 30 0 30 0
NAC (mM) - - + +
(F)
MCF-7R
P-gp
170 KD
GAPDH
36 KD
Relative mRNA level (P-gp)
12
9
6
3
0
***
***
***
Met (mg/L) 30 150 150 150 150
H2O2 (mM) 0 0 0.5 1.0 2.0
(G)
MCF-7S
Met (mg/L) 30 0 0
NAC(mM) - - +
(H)
MCF-7R
Met (mg/L) 30 150 150 150 150
H2O2 (mM) 0 0 0.5 1.0 2.0

Figure 3

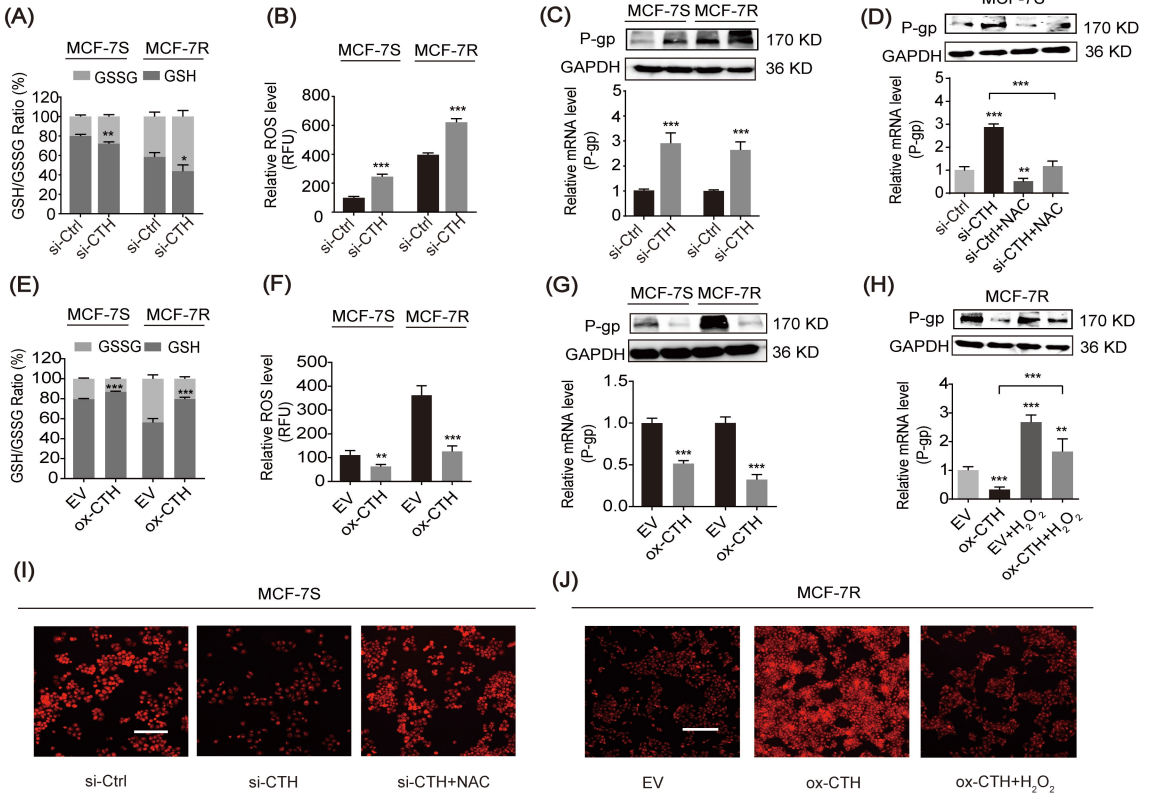
(A)
MCF-7S
MCF-7R
GSSG
GSH
GSH/GSSG Ratio (%)
si-Ctrl
si-CTH
(B)
Relative ROS level (RFU)
(C)
P-gp
170 KD
GAPDH
36 KD
Relative mRNA level (P-gp)
(D)
si-CTH+NAC
(E)
EV
ox-CTH
(F)
(G)
(H)
EV+H2O2
ox-CTH+H2O2
(I)
si-CTH+NAC
(J)

Figure 4

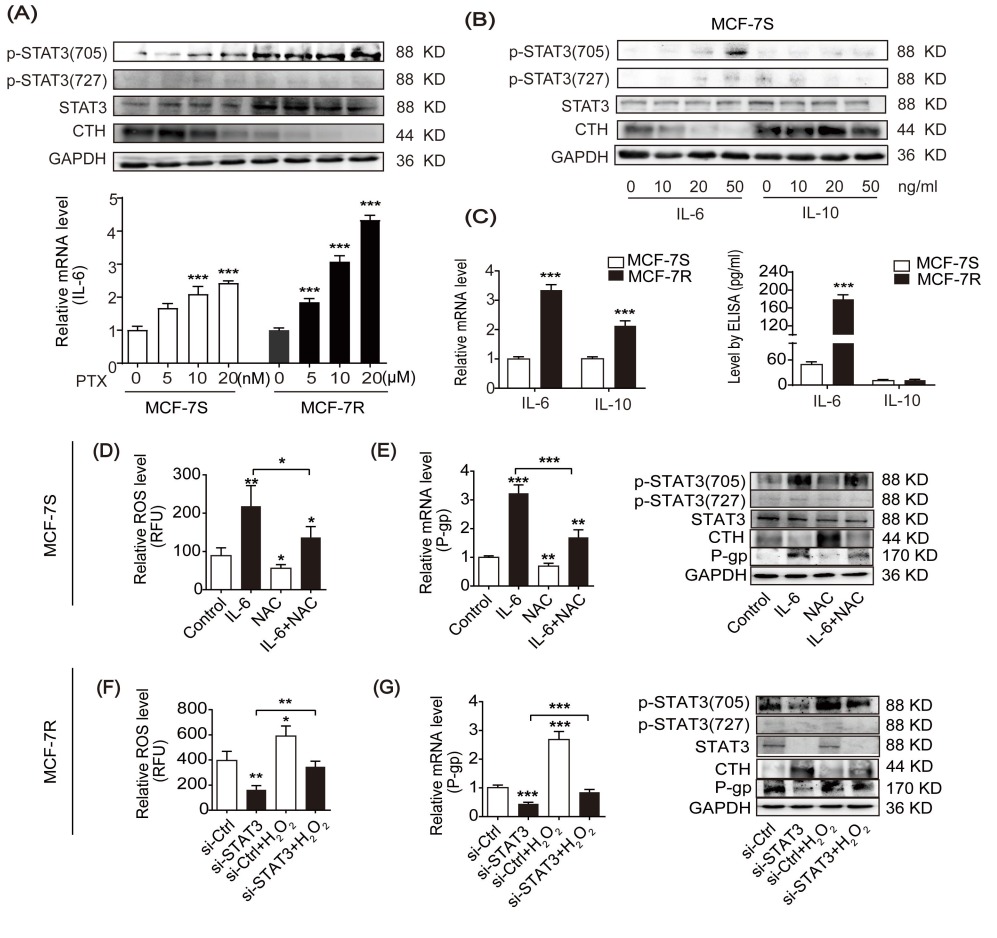
(A)
p-STAT3(705)
p-STAT3(727)
STAT3
CTH
GAPDH
88 KD
88 KD
88 KD
44 KD
36 KD
Relative mRNA level (IL-6)
PTX
0 5 10 20(nM) 0 5 10 20(μM)
MCF-7S
MCF-7R
(B)
MCF-7S
0 10 20 50 0 10 20 50 ng/ml
IL-6
IL-10
(C)
MCF-7S
MCF-7R
Relative mRNA level
Level by ELISA (pg/ml)
IL-6
IL-10
(D)
MCF-7S
Relative ROS level (RFU)
Control
IL-6
NAC
IL-6+NAC
(E)
Relative mRNA level (P-gp)
p-STAT3(705)
p-STAT3(727)
STAT3
CTH
P-gp
GAPDH
88 KD
88 KD
88 KD
44 KD
170 KD
36 KD
(F)
MCF-7R
Relative ROS level (RFU)
si-Ctrl
si-STAT3
si-Ctrl+H2O2
si-STAT3+H2O2
(G)
Relative mRNA level (P-gp)

Figure 5

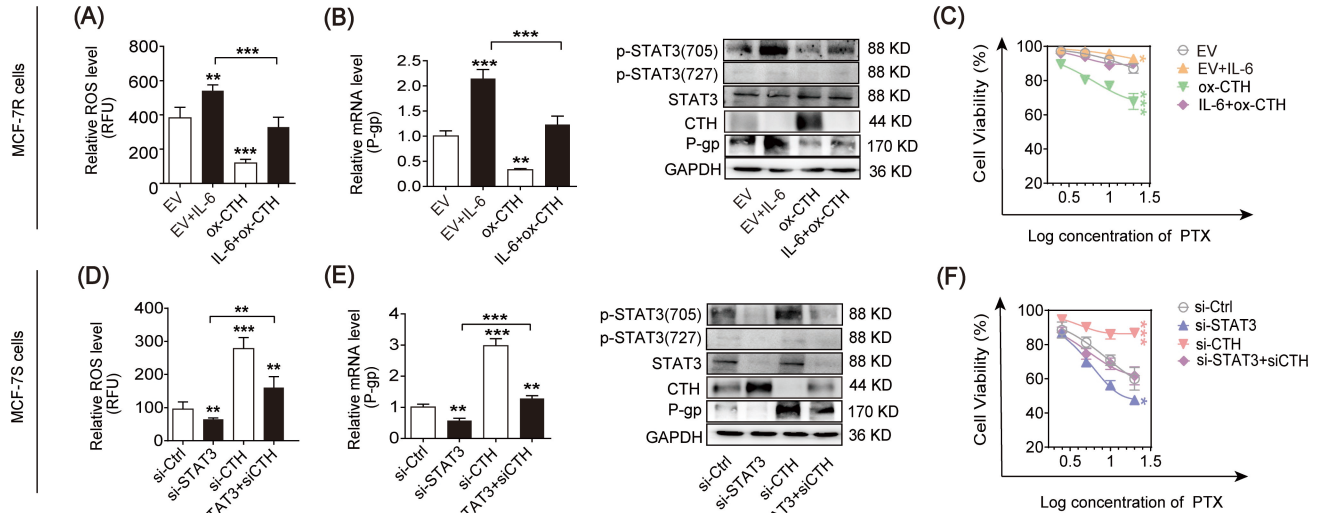
MCF-7R cells
(A)
Relative ROS level (RFU)
800
600
400
200
0
**
***
***
EV
EV+IL-6
ox-CTH
IL-6+ox-CTH
(B)
Relative mRNA level (P-gp)
2.5
2.0
1.5
1.0
0.5
0.0
***
***
**
EV
EV+IL-6
ox-CTH
IL-6+ox-CTH
p-STAT3(705)
p-STAT3(727)
STAT3
CTH
P-gp
GAPDH
88 KD
88 KD
88 KD
44 KD
170 KD
36 KD
EV
EV+IL-6
ox-CTH
IL-6+ox-CTH
(C)
Cell Viability (%)
100
80
60
40
20
0.5
1
1.5
Log concentration of PTX
EV
EV+IL-6
ox-CTH
IL-6+ox-CTH
MCF-7S cells
(D)
Relative ROS level (RFU)
400
300
200
100
0
**
**
***
**
si-Ctrl
si-STAT3
si-CTH
si-STAT3+siCTH
(E)
Relative mRNA level (P-gp)
4
3
2
1
0
***
***
**
**
si-Ctrl
si-STAT3
si-CTH
si-STAT3+siCTH
p-STAT3(705)
p-STAT3(727)
STAT3
CTH
P-gp
GAPDH
88 KD
88 KD
88 KD
44 KD
170 KD
36 KD
si-Ctrl
si-STAT3
si-CTH
si-STAT3+siCTH
(F)
Cell Viability (%)
100
80
60
40
20
0.5
1
1.5
Log concentration of PTX
si-Ctrl
si-STAT3
si-CTH
si-STAT3+siCTH

Figure 6

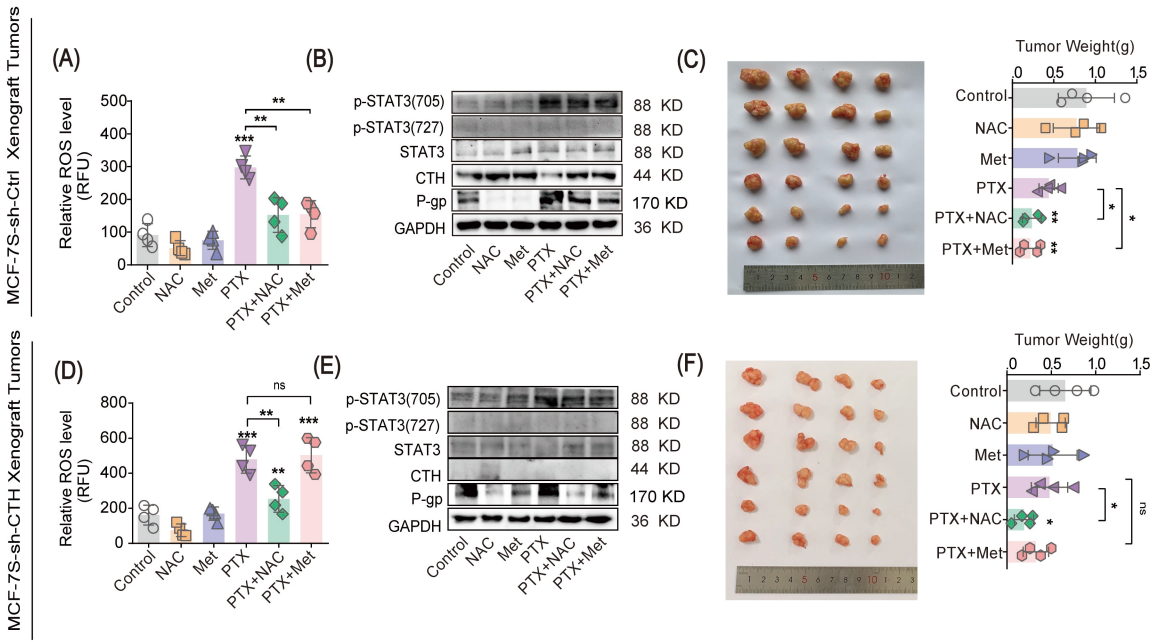
MCF-7S-sh-Ctrl Xenograft Tumors
(A)
Relative ROS level (RFU)
500
400
300
200
100
0
***
**
**
Control
NAC
Met
PTX
PTX+NAC
PTX+Met
(B)
p-STAT3(705)
p-STAT3(727)
STAT3
CTH
P-gp
GAPDH
88 KD
88 KD
88 KD
44 KD
170 KD
36 KD
Control
NAC
Met
PTX
PTX+NAC
PTX+Met
(C)
Tumor Weight(g)
0
0.5
1.0
1.5
Control
NAC
Met
PTX
PTX+NAC
PTX+Met
*
**
*
MCF-7S-sh-CTH Xenograft Tumors
(D)
Relative ROS level (RFU)
800
600
400
200
0
ns
**
***
**
***
Control
NAC
Met
PTX
PTX+NAC
PTX+Met
(E)
p-STAT3(705)
p-STAT3(727)
STAT3
CTH
P-gp
GAPDH
88 KD
88 KD
88 KD
44 KD
170 KD
36 KD
Control
NAC
Met
PTX
PTX+NAC
PTX+Met
(F)
Tumor Weight(g)
0
0.5
1.0
1.5
Control
NAC
Met
PTX
PTX+NAC
PTX+Met
*
*
ns